

CHAPTER 5

5. BACKCALCULATION OF THE CAPPING LAYER MATERIAL PROPERTIES

5.1 Introduction

This Chapter describes the application of the finite element model defined in Chapter 4 to determine the elasto-plastic properties of the capping layer material whose response to prescribed penetration in a semi-confined cylinder test (SCT) setup had been experimentally investigated as reported in Chapter 3. The properties were determined using a trial and error approach “backcalculation” process. As described in Chapter 3, the experimental data were grouped based on the level of moisture in the test specimens and the three groups of data thus formed were used in the backcalculation process. Each group consisted of the dataset from specimens tested under varying rates (2.5 – 25mm/min) and types (monotonic/ cyclic) of loading. This Chapter first describes the backcalculation process applied to the SCT setup, and then presents the properties of the capping layer material predicted from the simulations and compares the results with the reported values in the literature as well as that evaluated from a limited number of triaxial and uniaxial tests conducted as part of this thesis. The relevant data sheets of this Chapter are provided in Appendices C.1-C.10.

APPENDIX C.1	Density and saturation calculations-triaxial test samples
APPENDIX C.2	Triaxial test data sheets
APPENDIX C.3	Modulus, cohesion and friction angle obtained from triaxial tests
APPENDIX C.4	Uniaxial test data sheets
APPENDIX C.5	Density, saturation, initial modulus and hardening modulus - uniaxial test samples
APPENDIX C.6	Establishing lower and upper boundaries of SCT data
APPENDIX C.7	Effect of moisture on SCT FEM predicted parameters

APPENDIX C.8	Sensitivity of elastic material parameters in SCT FEM
APPENDIX C.9	Sensitivity of plastic material parameters in SCT FEM
APPENDIX C.10	Stresses induced in SCT FEM

5.2 Backcalculation Process

Backcalculation process has briefly been reviewed in Chapter 2. This process is also referred to as inverse method in the literature. Inverse method is a term for the determination of material properties from structural response data. Traditionally material properties are determined from small size specimens tested under uniform state of stress, most commonly uniaxial compression or tension. The properties evaluated using such simple test methods do not always provide accurate predictions of the behaviour of structures especially under complex states of loading. Furthermore, with the advent of new materials, especially composites, it becomes increasingly difficult to use such simple test methods to determine the properties of materials. Therefore there is a growing modern trend of using inverse method (Kang et al. 2004; Lin et al. 2005) to determine material properties from structural response determined experimentally (and hence the term “inverse method”). These inverse methods invariably use FE modelling combined with some advanced search techniques for example, Genetic Algorithm or GA (Lin et al. 2005) to determine the most appropriate material dataset to satisfy the observed structural behaviour.

As soils are complex media with significant variability of their properties, it was decided not to use very sophisticated search techniques such as the GA for material dataset determination – but rather limit the search to some indicative upper and lower bound values using trial and error method known as the backcalculation procedure.

The structural behaviour observed from the SCT specimens are shown in Fig. 5.1 as three distinctive groups of dry, OMC and saturated data.

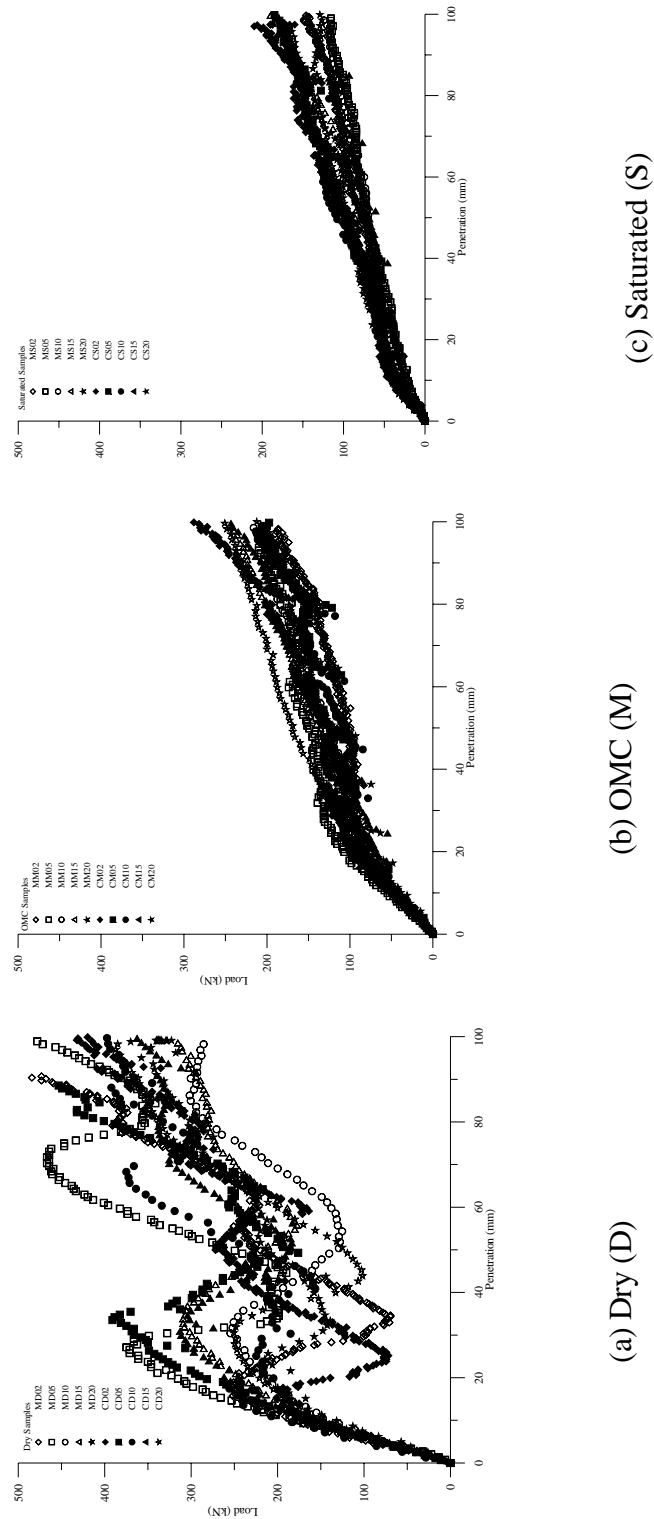


Figure 5.1 Three distinctive groups of experimental data obtained from SCT

Estimating the upper and lower bounds of material properties for these three groups was considered sufficient given the variability in soil behaviour observed in the field. Although deformation of about 20-30mm is considered a failure in practice for railway subgrades, we have considered a penetration of up to 100mm to improve the reliability of the evaluated material property datasets.

Eleven user input parameters describe the behaviour of the capping layer material adequately. They are:

- the minimum elastic modulus (E_0),
- the maximum elastic modulus (E_{max}),
- the Poisson's ratio (ν),
- the minimum friction angle (ϕ_{min}),
- the maximum friction angle (ϕ_{max}),
- the cohesion (c),
- the dilatancy angle (ψ),
- the hardening parameter (H_p),
- the factor (R_f) and
- the two material constants (K_a) and (n)

The above user inputs are then classified as elastic or plastic parameters as shown in Table 5.1. Multiple combinations of the user inputs in Table 5.1 can be applied in the simulation process, which will lead to a considerable number of trial runs in the analysis. Thus, to simplify the simulation process, values suggested in the literature and material parameters obtained from triaxial/uniaxial tests on the capping layer material were used as a guide and they were classified further as primary, secondary or tertiary parameters.

Table 5.1 User input parameters

Elastic	Plastic
$E_0 \leq E_t \leq E_{\max}$ (MPa)	ψ ($^{\circ}$)
$\phi_{\min} \leq \phi \leq \phi_{\max}$ ($^{\circ}$)	
c (MPa)	H_p (MPa)
ν	
K_a	R_f
n	

The direct measurement of ν is very difficult and suggested values of other references are generally considered acceptable in geotechnical engineering (Liao 2003). A value for ν of 0.3 was suggested by Croney and Croney (1992) for unbound base and sub-base materials in pavements while for sand and gravelly sand the most commonly used value range for ν was between 0.3 - 0.4 (Bowles 1988). Although with the increase in stress level the Poisson's ratio, ν could increase (Croney and Croney 1992; Lambe and Whitman 1979), ν was kept a constant at 0.35 in all simulations for simplification, which is representative enough for the capping layer material used in the experiments being a mixture of very sandy gravel with a feeble plastic binder (refer Section 3.3).

The values suggested in literature specify the range of 0.7-0.9 for R_f (Desai and Christian 1977). Thus, it was decided to keep R_f constant at 0.8 simplifying the backcalculation process.

The dilatancy angle ψ was not measured for the material; it was decided to use values suggested in the literature as a guide to find a specific range in the simulations. According to Liao (2003) the values of ψ suggested by Vermeer and de Borst in 1984 are given in Table 5.2.

Table 5.2 Values of dilation angle (ψ) suggested by Vermeer and de Borst in 1984 (Liao 2003)

Dense sand	15^0
Loose sand	$<10^0$

Liao (2003) also stated that these values were broadly suggested in geotechnical computer software like FLAC^{3D} and PLAXIS, and further stated that a simple empirical equation was suggested in the programs given by:

$$\psi = \phi - 30^0. \quad (5.1)$$

The theoretical solutions stated by Liao (2003) are:

Maximum theoretical dilation angle suggested by Bolton (1986) for plane strain conditions

$$\sin \psi_{\max} = \left[\frac{-(d\varepsilon_1 + d\varepsilon_3)}{(d\varepsilon_1 - d\varepsilon_3)} \right]_{\max} \quad (5.2)$$

where ε_1 = axial strain and ε_3 = lateral strain and

Maximum theoretical dilation angle suggested by Tatsuoka (1987) for triaxial conditions

$$\sin \psi_{\max} = \left[\frac{-(d\varepsilon_1 / 2 + d\varepsilon_3)}{(d\varepsilon_1 / 2 - d\varepsilon_3)} \right]_{\max} \quad (5.3)$$

If Eqn. (5.1) is used in calculating ψ , the corresponding values for $\phi = 30^0, 35^0$, and 40^0 would be $0^0, 5^0$ and 10^0 respectively.

Thus, by considering the suggested values it was decided to employ $\psi < 15^0$ in the simulation process.

The two material constants K_a and n were calibrated using a limited set of drained triaxial tests taking the reference pressure p_a as 100kPa (normal practice is to choose a value close to the atmospheric pressure of 101kPa). The triaxial results were also used to

identify possible ranges for the user inputs of E_t , ϕ , and c . Uniaxial tests were carried out to find possible ranges of values for E_0 and H_p . The following describes the triaxial and uniaxial tests carried out.

Triaxial and Uniaxial Test Data

a) Triaxial tests

The triaxial tests carried out served four purposes, (i) calibration of model parameters K_a and n , (ii) deriving an equation to use in the subroutine for the stress dependent friction angle, (iii) use of extracted values E_t , c and ϕ as a preliminary guide to initial inputs in the trial simulations and (iv) comparison with model backcalculation predictions. A set of standard drained triaxial tests (AS 1289.6.4.1. 1998; AS 1289.6.4.2 1998; Bishop and Henkel 1962) for the loading rates (2.5, 5.0, 10.0, 15.0 and 20mm/min) considered in the SCT for confining pressures below 800kPa were carried out at the Central Queensland University (CQU). The tests were carried out for 100, 375 and 750kPa confining pressures. Another set of tests at 2.5mm/min for higher confining pressures of 1000 and 2000kPa were carried out at the University of Sydney (USyd). Higher levels of confining pressure were not possible at CQU and higher levels of rate of loading were not possible within the time available at USyd. Further details and data of triaxial tests are contained in Appendices C.1-C.3.

200mm high x 100mm diameter samples were used for testing. The samples were prepared using modified compactive effort (AS 1289.6.8.1 1995). The samples were compacted in five layers, each of about 40 mm thick subjected to 56 blows with the 4.9kg Proctor hammer falling a distance of 450mm.

Fig. 5.2 shows the setup used at CQU and USyd. The 2.5mm/min rate data was used in calibrating the model parameters K_a and n as the confining pressure range 100-2000kPa best represents the high confining stresses induced in the SCT. The initial modulus, cohesion and friction angle obtained from the triaxial tests are given in Table 5.3 while the average values are used in Table 5.11 for comparisons.



(a) CQU apparatus

(b) USyd apparatus

Figure 5.2 Triaxial setup

Table 5.3 Material properties obtained from triaxial tests

Material property	Confining pressure (kPa)	Deformation rate (mm/min)					Average
		2.5	5.0	10.0	15.0	20.0	
E_t (MPa)	100	88	106	111	125	112	108
	375	260	283	266	282	256	269
	750	360	414	392	372	366	381
	1000	479	-	-	-	-	479
	2000	589	-	-	-	-	589
c (kPa)	100-750	263	323	356	315	391	330
	1000-2000	534	-	-	-	-	534
ϕ^0 (deg)	100-750	38	40	38	38	39	39
	1000-2000	36	-	-	-	-	36

The calibration of K_a and n is shown in Fig. 5.3. By comparison of the best-fit power curve of the data and Eqn. (4.43) as shown in Fig. 5.3, the values evaluated and used in the analysis for K_a and n are 970 and 0.65 respectively.

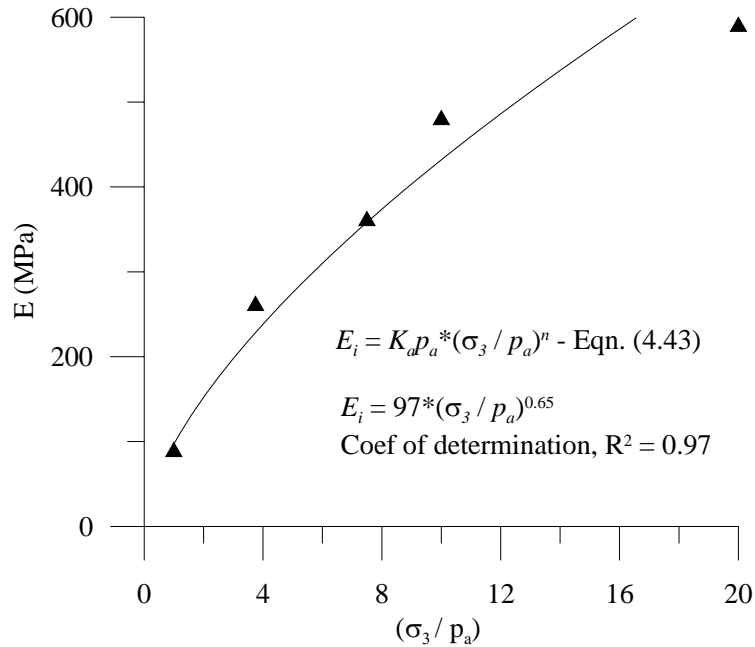


Figure 5.3 Calibration of K_a and n

Obtaining a possible relationship for the stress dependency of the friction angle was also carried out using the triaxial test results. Table 5.4 presents the data used in deriving the stress dependent friction angle (Eqn. 4.51) described in Section 4.3.2.

Table 5.4 Variation in ϕ at different stress levels

Confining pressure σ_3 (kPa)	Average confining pressure σ_3 (kPa)	Major principal stress at failure $(\sigma_1)_f$ (kPa)	Average principal stress at failure $(\sigma_1)_f$ (kPa)	$(\sigma_1 / \sigma_3)_f$	Friction angle ϕ^0 (deg)
100-375	238	1900 -3579	2739	11.5	46
375-750	563	3579-5300	4439	7.9	40
1000-2000	1500	6004-9900	7952	5.3	36

b) Uniaxial compression tests

The uniaxial compression tests (see Fig. 5.2a) were carried out to find a suitable input range for the minimum elastic modulus E_0 and the hardening modulus H_p of the

material. Two uniaxial compression tests on OMC samples were carried out (AS 1141.51 1996; AS 4133.4.2 1993). Fig. 5.4 shows the effective stress-effective strain of the material showing H_p for the material. The results obtained for E_0 and H_p are shown in Table 5.5. Accordingly for the capping layer material at OMC state, $E_0 = 25\text{MPa}$ and $H_p = 270\text{kPa}$. Appendices C.4 and C.5 present the detail data of the uniaxial compression tests.

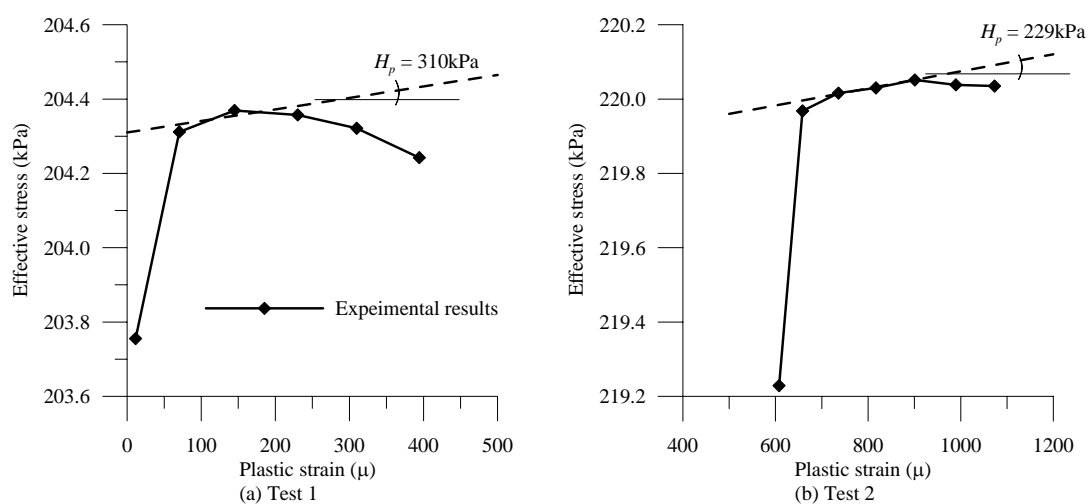


Figure 5.4 Effective stress-effective strain curves of the OMC samples

Table 5.5 E_0 and H_p of the capping layer material at OMC state

	E_0 (MPa)	H_p (kPa)
Test 1	27	310
Test 2	22	229
Average	25	270

From the triaxial and uniaxial tests data, suitable ranges for input values for numerical simulations would be $E < 600\text{MPa}$, ϕ between 30^0 - 40^0 , $c < 1\text{MPa}$ and $H_p < 1\text{MPa}$.

Based on the above discussion and the importance of definitions used in the constitutive relationships the above inputs were categorised as primary, secondary or tertiary parameters as shown in Table 5.6.

Table 5.6 Classification of user input parameters as primary, secondary or tertiary

Elastic Parameters		Plastic Parameters	
$E_0 \leq E_t \leq E_{\max}$ (MPa)	Primary	ψ ($^{\circ}$)	Primary
$\phi_{\min} \leq \phi \leq \phi_{\max}$ ($^{\circ}$)	Primary		
c (MPa)	Secondary	H_p (MPa)	Secondary
ν	Tertiary		
K_a	Tertiary	R_f	Tertiary
n	Tertiary		

Thus, the backcalculation process was much simplified by keeping the tertiary parameters constant and varying only the primary and secondary parameters. The following summarises the final conclusions drawn on the simplification of simulation process.

- Keep K_a (= 970) and n (= 0.65) constant in all simulations obtained through triaxial tests taking the reference pressure p_a as 100kPa.
- Keep ν (= 0.35) and R_f (= 0.8) constant in all simulations considering the relevant suggestions in literature.
- Keep the secondary parameters $c < 1\text{MPa}$, and $H_p < 1.0\text{MPa}$ in all simulations considering the values obtained from triaxial/uniaxial test data.
- Keep the primary parameters $E < 750\text{MPa}$, ϕ between $30^{\circ} - 40^{\circ}$, and $\psi < 15^{\circ}$ considering the triaxial test data and suggestions made in literature respectively.
- Main parameters to be changed in the simulation process to match the upper and lower bound envelopes of the experimental data are the primary elastic parameters E_t , ϕ and plastic parameter ψ .
- The values obtained for the primary parameter ϕ in matching the lower bound to be employed in matching the upper bound.
- The values employed for the secondary parameters c and H_p in matching upper bound to be kept close to the values obtained from lower bound simulations.

The flow chart for the adopted simulation process is summarised in Fig. 5.5.

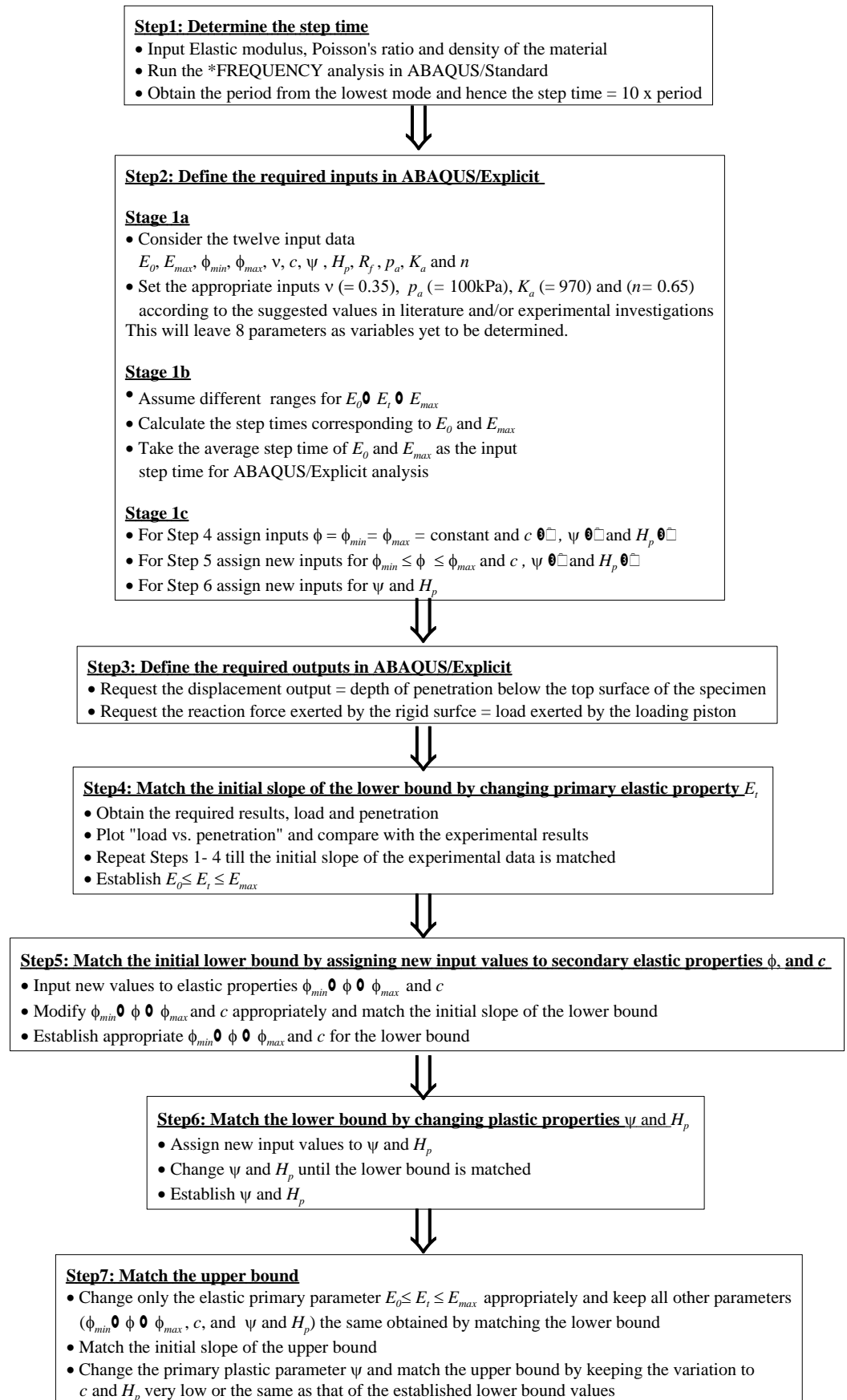


Figure 5.5 Flow chart of simulation process

5.2.1 Results of the ABAQUS Simulations

5.2.1.1 Model Predictions – OMC State (M)

The most representative envelopes obtained from the simulations are shown in Fig. 5.6 for OMC state specimens. The model predicted the response reasonably well for a penetration level up to 80mm which is about 45% of the total height of 177.5mm of the SCT setup. In fact the model was able to predict the properties for a broad range of confining stress levels providing more valuable data.

The inability of the model to capture the remoulding behaviour beyond 80mm penetration level was considered not very significant. Firstly the choice of 100mm is arbitrary and somewhat extreme from practical perspective. The simplified trial and error based backcalculation process could possibly have limitations in determining the appropriate dataset for the behaviour of material at highly nonlinear condition.

The model predicted properties are given in Table 5.7 for the OMC state of the material.

Table 5.7 Model predicted properties – OMC state

		Elastic Parameters			Plastic Parameters	
		$E_0 \leq E_t \leq E_{\max}$ (MPa)	$\phi_{\min} \leq \phi \leq \phi_{\max}$ ($^\circ$)	c (kPa)	ψ ($^\circ$)	H_p (kPa)
OMC	Lower bound	$30 \leq E_t \leq 80$	$35 \leq \phi \leq 38$	300	4	300
	Upper bound	$80 \leq E_t \leq 130$	$35 \leq \phi \leq 38$	350	7	350

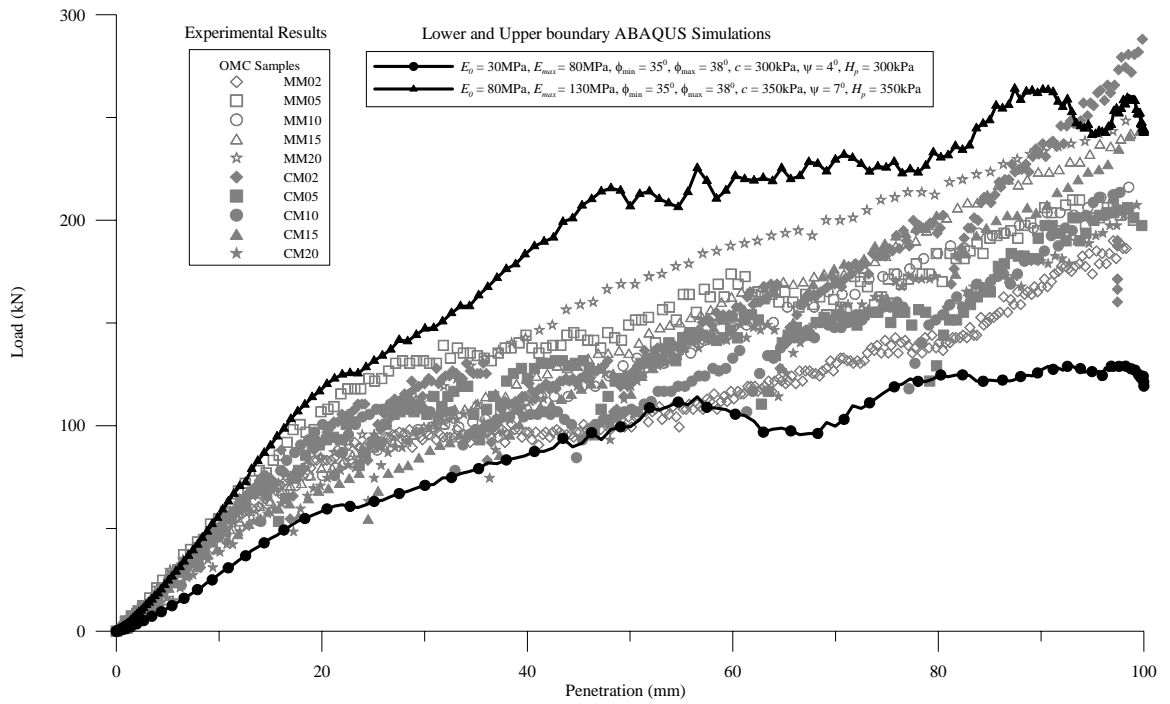


Figure 5.6 Predicted boundary envelopes of OMC state

5.2.1.2 Model Predictions – Saturated State (*S*)

Similar to the OMC state specimens the saturated state specimen properties were also predicted reasonably well up to 80mm penetration level by the FE based backcalculation process. Beyond 80mm penetration level the prediction was not completely satisfactory. The model predictions are given in Table 5.8 while Fig. 5.7 shows the predicted boundary envelopes.

Table 5.8 Model predicted properties – Saturated state

		Elastic Parameters			Plastic Parameters	
		$E_0 \leq E_t \leq E_{\max}$ (MPa)	$\phi_{\min} \leq \phi \leq \phi_{\max}$ ($^\circ$)	c (kPa)	ψ ($^\circ$)	H_p (kPa)
Saturated	Lower bound	$20 \leq E_t \leq 45$	$33 \leq \phi \leq 35$	300	7.5	300
	Upper bound	$55 \leq E_t \leq 80$	$33 \leq \phi \leq 35$	300	6.7	300

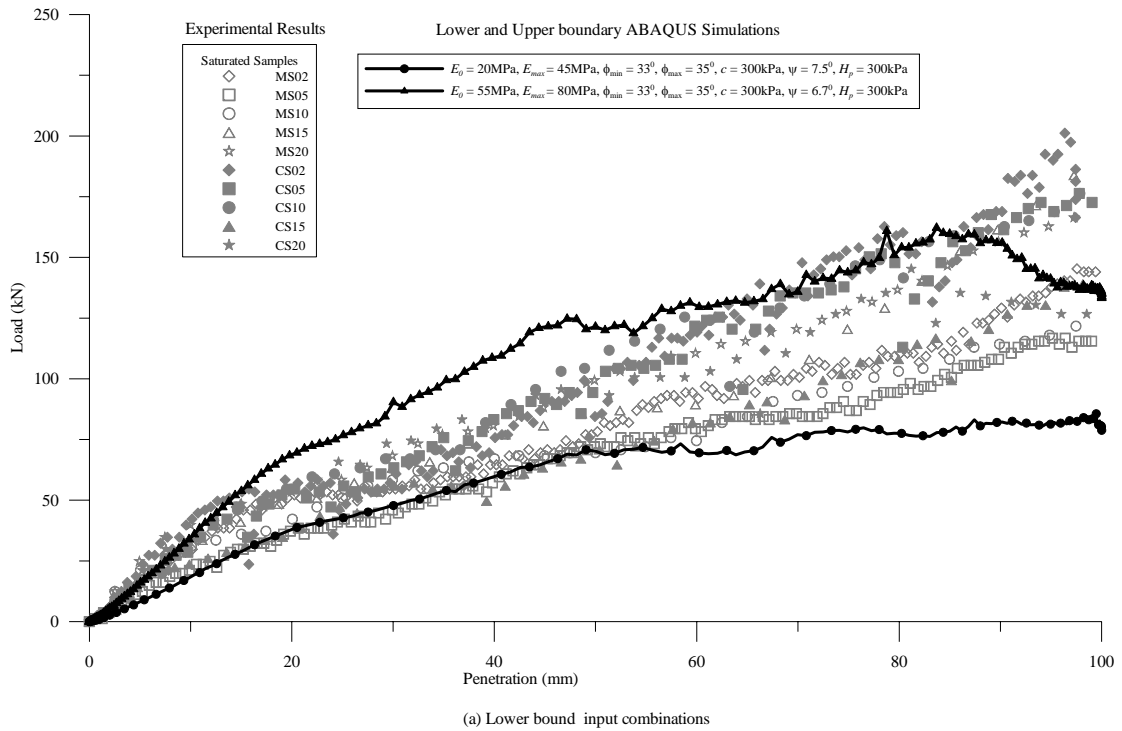


Figure 5.7 Predicted boundary envelopes of saturated state

5.2.1.3 Model Predictions – Dry State (D)

The hardening-failure-remoulding behaviour of the dry state specimens was very much pronounced compared to that of the OMC and saturated states of the material. The model was not capable of predicting the zigzag behaviour observed in the experiments in its present form. The absence of moisture in dry specimens makes them a separate class as presented in Chapter 3 (see dimensional analysis and ternary plot sections). Therefore, conservative lower and upper boundaries were obtained via the backcalculation process capturing all the variations as shown in Fig. 5.8. Table 5.9 shows the results of the simulated boundaries. The broad variation (upper bound is about 4 times the lower bound) in the dataset may not represent true material behaviour and based on the limitations of the current model, the dataset presented in Table 5.9 should be considered with caution.

The increase in stiffness and brittleness suggests that the cohesion ‘*c*’ plays a more dominant role in the failure-remoulding behaviour of the dry specimens. Developing a backcalculation process for determination of dry specimen material dataset requires very intensive research and hence is not considered further in this thesis.

Table 5.9 Model predicted properties – Dry state

		Elastic Parameters			Plastic Parameters	
		$E_0 \leq E_t \leq E_{\max}$ (MPa)	$\phi_{\min} \leq \phi \leq \phi_{\max}$ ($^\circ$)	<i>c</i> (kPa)	ψ ($^\circ$)	H_p (kPa)
Dry	Lower bound	$80 \leq E_t \leq 100$	$40 \leq \phi \leq 43$	200	2	200
	Upper bound	$345 \leq E_t \leq 350$	$40 \leq \phi \leq 43$	200	2	200

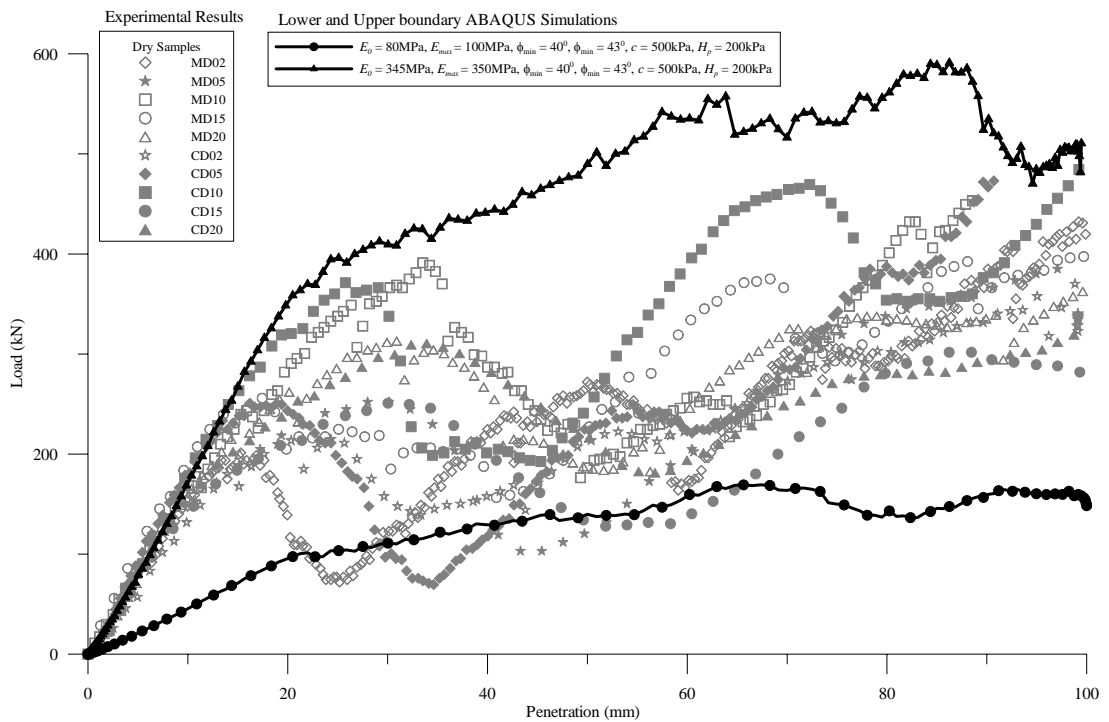


Figure 5.8 Predicted boundary envelopes of dry state

5.2.1.4 Final Output

Table 5.10 summarises the material properties predicted from simulations of the OMC, saturated and dry states of the experimental data. The relevant FE simulation data are provided in Appendix C.6.

Table 5.10 Predicted material properties from simulations

		Elastic Parameters			Plastic Parameters	
		$E_0 \leq E_t \leq E_{\max}$ (MPa)	$\phi_{\min} \leq \phi \leq \phi_{\max}$ ($^{\circ}$)	c (kPa)	ψ ($^{\circ}$)	H_p (kPa)
Dry	Lower bound	$80 \leq E_t \leq 100$	$40 \leq \phi \leq 43$	500	2	200
	Upper bound	$345 \leq E_t \leq 350$	$40 \leq \phi \leq 43$	500	2	200
OMC	Lower bound	$30 \leq E_t \leq 80$	$35 \leq \phi \leq 38$	300	4	300
	Upper bound	$80 \leq E_t \leq 130$	$35 \leq \phi \leq 38$	350	7	350
Saturated	Lower bound	$20 \leq E_t \leq 45$	$33 \leq \phi \leq 35$	300	7.5	300
	Upper bound	$55 \leq E_t \leq 80$	$33 \leq \phi \leq 35$	300	6.7	300

As expected from the experimental results, the saturated state had the lowest values of the elastic properties, E_0 , E_{\max} , ϕ_{\min} and ϕ_{\max} for each of the lower and upper bound while the dry state showed the highest values. The plastic modulus was the same for both saturated and OMC states while dry state predictions were the lowest.

The lowest range between $E_0 = 345$ MPa and $E_{\max} = 350$ MPa was observed in the upper bound at the dry state while the highest range was observed in the OMC state. A similar pattern was observed in the lower bound values of E_0 and E_{\max} too. These ranges show the variability expected from the simulations which are relevant to critical soil conditions, in the present case mainly the degree of saturation and the very high stress levels.

Friction angle and tangent modulus are primary strength indices for soils. The initial tangent modulus is more influential in obtaining better analytical results. Table 5.11 shows some typical values suggested in literature for E , ϕ , ν , ψ and c , for soils of similar type to the capping layer material.

Budhu (2000) and Duncan (1992) have indicated typical values of peak friction angle ϕ_p and the ultimate friction angle ϕ_{cv} for mixtures of gravel and sands with fine grained soils

(Liao 2003). Further, empirical equations of friction angle for granular soils can be found in Liao (2003). The ϕ values predicted from the model of $33^{\circ} - 43^{\circ}$ are justifiable compared to the values suggested for mixtures of gravel and sands with fine grained soils. As discussed by Means and Parcher (1964), the angle of friction ϕ' exhibited by the naturally or artificially cemented granular soil is smaller than that of the friction angle ϕ exhibited by the same soil in an uncemented state (Fig. 5.9). They further stated that a cemented material undergoes two failures, one when the cohesive resistance is broken and again when the internal shearing resistance of the granular component is broken. The strain required to develop the full shearing resistance is much greater than that required to break the cohesive bonds. Line AD represents the strength of soil at the instant when cohesive bonds are just about to be broken and line OC shows the shearing resistance at much larger strains when complete destruction of the bonds of the cementation material has occurred and material behaviour is similar to that of a clean granular soil. As such, comparison of the current model predicted data with triaxial test data are also presented in Table 5.11.

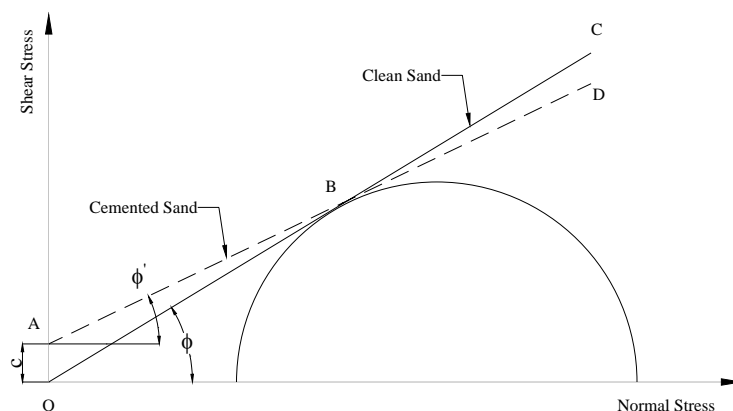


Figure 5.9 Strength line of cemented granular soils (Means and Parcher 1964)

Typical modulus values suggested for different types of soils are presented in Table 5.11. A comprehensive study of various empirical relationships suggested in literature can be

found in Liao (2003). The model predicted E_0 values of 20-55MPa for saturated state, 30-80MPa for OMC state and 80-345MPa for dry state and E_{max} values of 45-80MPa for saturated state, 80-130MPa for OMC state and 100-350MPa seem reasonable when compared with the values for sand and gravel and the values obtained from the triaxial test results in Table 5.11. Further, in comparison to the uniaxial test results of the OMC state samples, the model predictions of saturated and OMC states seem reasonable.

For sub-base and unbound base materials used in pavements, the following values were suggested by Croney and Croney (1992) as useful target values in structural analysis. An initial modulus of 150MPa with a ν of 0.3 was suggested for the unbound base and a modulus of 100-150MPa for the sub-base (Croney and Croney 1992). Sowers (1979) also discussed that ν is not a constant and is stress dependent. Sowers (1979) stated that ν exceeds 0.5 when the volume and void ratio of a dense cohesionless soil increase as the peak strength is reached. Some typical values of ν are given in Table 5.11. Accordingly, for sands and gravelly sands ν varies from 0.1 to 1.0, while the commonly used value is between 0.3- 0.4. Some empirical relationships synthesised in the past also can be found in Liao (2003). Therefore the assumed value of 0.35 is reasonable and representative enough in predicting other material parameters from the model.

As already discussed in choosing the value of $\psi < 15^0$, the predicted values $< 7.5^0$ seem reasonable.

Croney and Croney (1992) also indicated that use of high modulus values leads to the prediction of significant tensile stresses in the unbound material ($< 10\text{kPa}$), and suggest a

stress-dependent modulus be used so that tensile stresses in excess of 10kPa are not predicted. In order to prevent excessive tensile stresses, a tension cut-off can be incorporated in the model.

Table 5.11 Comparison of model predicted data with published, triaxial and uniaxial test data

Properties obtained from model predictions (This Thesis)								
	Elastic properties					Plastic properties		
	Modulus, E (MPa)		Poisson's ratio, ν	Friction angle, ϕ ($^\circ$)		Cohesion, c (kPa)	Dilation angle, ψ ($^\circ$)	Hardening Modulus, H_p (kPa)
	E_0	E_{max}						
Dry state	80-345	100-350	Assumed as 0.35	40-43		~ 500	~ 2	~ 200
OMC state	30-80	80-130		35-38		300-350	4-7	300-350
Saturated state	20-55	45-80		33-35		~ 300	6.7-7.5	~ 300
Properties obtained from uniaxial test data (This Thesis)								
Unconfined test	25							270
Properties obtained from triaxial test data (This Thesis)								
Confining pressure	100kPa	108		39		330		
	375kPa	269						
	750kPa	381		36		534		
	1000kPa	479						
	2000kPa	589						
Published data for soils								
<i>Note: *Referenced in (Liao 2003)</i>								
Reference	Elastic properties					Plastic properties		
	Modulus, E (MPa)		Poisson's ratio, ν	Friction angle, ϕ ($^\circ$)		Cohesion, c (kPa)	Dilation angle, ψ ($^\circ$)	Hardening Modulus, H_p (kPa)
	*Cernica (1995)	*Bowels (1992)	Bowels (1998)	*Duncan (1992)	*Budhu (2000)		*Vermeer and de Borst (1992)	
Sand and Gravel Loose	100	50-150					<10	
Dense	150	100-200					15	
Sand, gravely sand			0.1-1.0					
Commonly used			0.3-0.4					
Mixtures of gravel and sand with fine grained soils				33-36 (peak)	28-33 (ultimate)	30-40 (peak)		

Figure 5.10 shows typical Mohr-Coulomb failure envelopes of the material tested. The material showed some cohesion and a high friction angle. By comparison, the final model backcalculation predicted results of modulus values in Table 5.11 seem well correlated

with the triaxial test results. The ϕ values of saturated samples are much lower than that obtained from the triaxial tests, the OMC and dry sample predictions are much more representative of triaxial data.

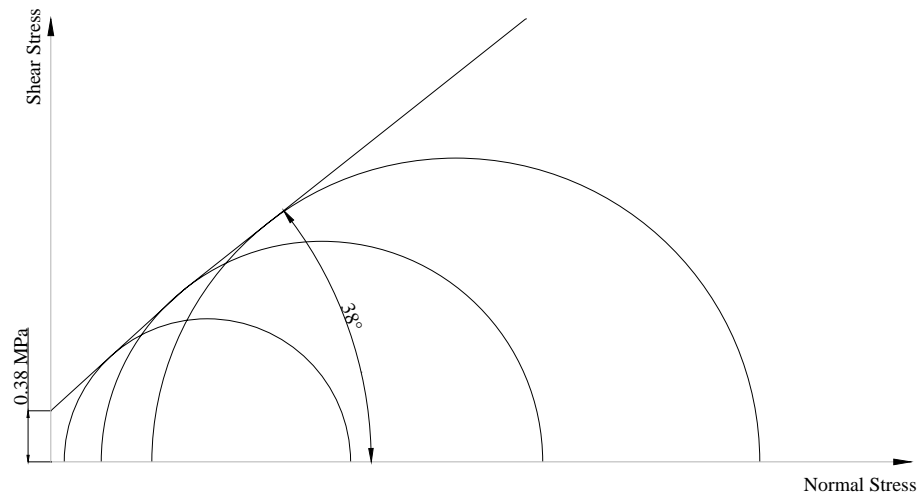


Figure 5.10 Typical Mohr-Coulomb envelopes of the material tested

From the foregoing discussion and Table 5.11 it can be concluded that the model backcalculation predictions are reasonable. The experimental and numerical investigations provided valuable qualitative and quantitative data over a wide range of stress levels.

5.2.2 Effect of Moisture Content on Predicted Parameters

From widely published data for unbound materials and all the experimental results and simulations obtained it was evident that the saturation level of the material governs the material properties. As such the effect of the moisture in dry, OMC and saturated states of the material is discussed below. The trends shown in Figs. 5.11-5.15 are very much dependant on dry state data and should be considered with caution. The relevant data sheets are located in Appendix C.7.

a) Effect on tangent modulus E_t

Fig. 5.11 shows the effect of moisture content on the predicted parameters of the material, E_0 and E_{max} . The predicted parameters show a range of modulus values which narrows down at the high moisture contents. Therefore it can be concluded that the tangent modulus obtained is very much sensitive to the moisture content.

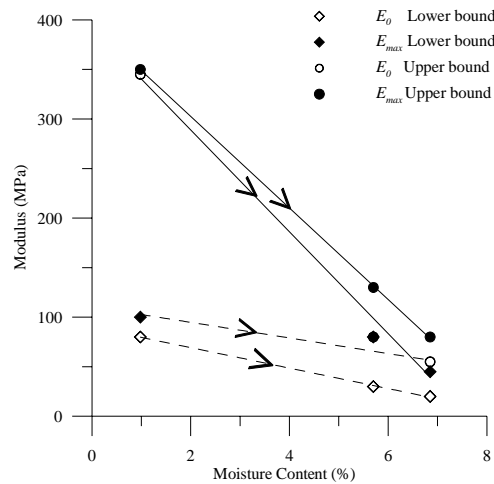


Figure 5.11 Effect of moisture on the tangent modulus

b) Effect on friction angle ϕ

Friction angle decreased with the increase in moisture, as apparent from Fig. 5.12.

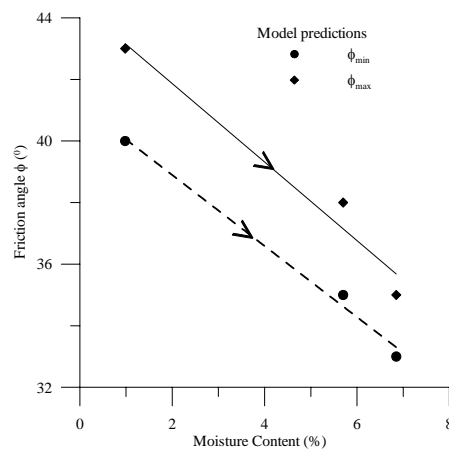


Figure 5.12 Effect of moisture on friction angle

c) Effect on cohesion c

Fig. 5.13 shows the effect of moisture on cohesion. As apparent from the model predictions the cohesion has increased with the decrease in moisture.

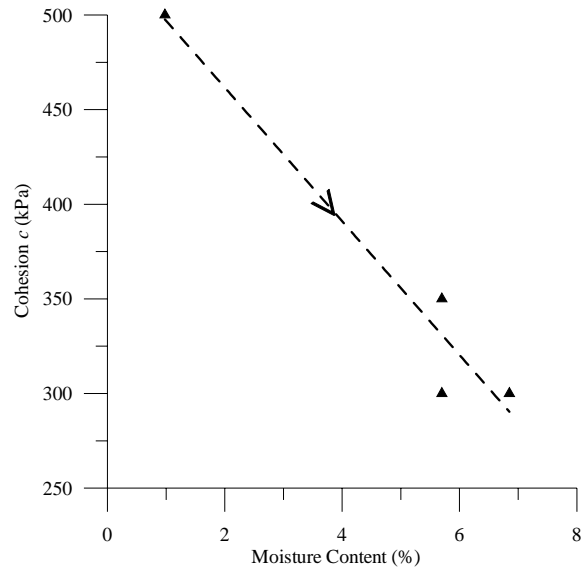


Figure 5.13 Effect of moisture on cohesion

d) Effect on dilation angle ψ

The predicted dilation angle showed an increase with the increase in the moisture content as shown in Fig. 5.14 whereas the friction angle showed the opposite trend (Fig. 5.12)

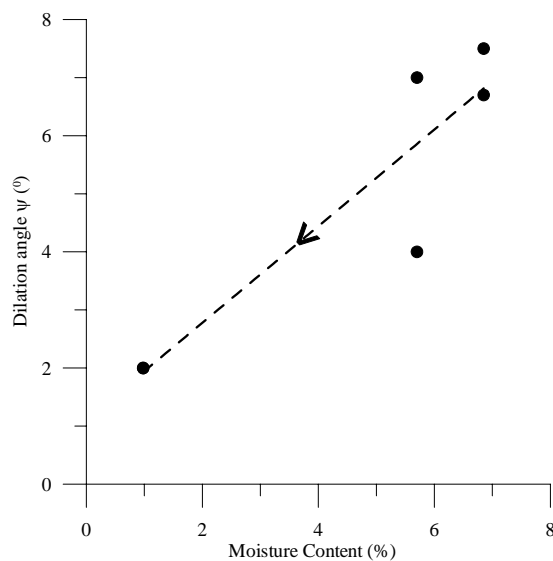


Figure 5.14 Effect of moisture on dilation angle

e) Effect on hardening modulus H_p

Hardening modulus also showed an increase with the increase in the moisture shown in Fig. 5.15. The hardening modulus itself has very low values (200-300kPa), thus its variation is not a very significant issue.

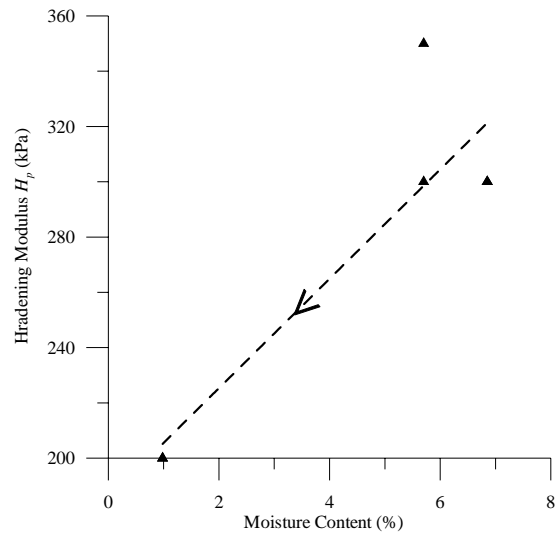


Figure 5.15 Effect of moisture on hardening modulus

Therefore it can be concluded that moisture has a greater effect on elastic material properties of tangent modulus, friction angle and cohesion, reducing them with the increase in the moisture content. On the other hand the plastic properties of dilation angle and the hardening modulus increased with the increase in the moisture. This may be caused due to the decrease in stability of the fine-grained components with the increase in moisture.

As discussed by Lambe and Whitman (1979), the friction between the mineral particles reduces with the introduction of water causing a decrease in shearing resistance as well as the friction angle. Al-Shayea (2001) has discussed that the properties of artificial clay-sand mixtures are highly influenced by the clay content and the moisture content. Al-Shayea (2001) has found that the internal frictional angle and shearing resistance generally

decreases with increasing water content or clay contents. This was very much observed in the experimental results (Fig. 5.1) as well as in the model prediction properties.

5.2.3 Parametric Study

In order to investigate the various assumptions made in the constitutive relationship and in modelling, a parametric study was performed considering the OMC predictions from the SCT model. The sensitivity analysis was performed individually for the primary parameters (E_t , ψ and ϕ) and the secondary parameters (c and H_p) to observe their degree of influence and significance on the variability of the load-penetration profiles obtained from the simulations of the SCT results. The medium mesh described in Section 4.1.7 was used in all the sensitivity analyses. The sensitivity of each selected parameter was analysed while keeping the input values of all other parameters at a prescribed level taken as the average for upper and lower bound of OMC state envelopes (Table 5.10) for simplicity here. The parameters varied in the sensitivity analysis are shown in the diagonal of Table 5.12 while the rest are the parameters whose values were fixed for the sensitivity studies. The relevant FE analysis data are provided in Appendices C.8 and C.9.

Table 5.12 Average parameter values of OMC state used in sensitivity analysis

$E_0 \leq E_t \leq E_{\max}$ (MPa)	$\phi_{\min} \leq \phi \leq \phi_{\max}$ ($^{\circ}$)	c (kPa)	ψ ($^{\circ}$)	H_p (kPa)
E_t	$35 \leq \phi \leq 38$	325	5.5	325
$55 \leq E_t \leq 105$	ϕ	325	5.5	325
$55 \leq E_t \leq 105$	$35 \leq \phi \leq 38$	c	5.5	325
$55 \leq E_t \leq 105$	$35 \leq \phi \leq 38$	325	ψ	325
$55 \leq E_t \leq 105$	$35 \leq \phi \leq 38$	325	5.5	H_p

1) Elastic parameters

The elastic parameters considered for the sensitivity analysis are E_t , ϕ and c .

The effect of tangent modulus E_t on the load-penetration response was investigated by:

- (i) keeping E_t (for two cases) as constant by considering the lowest and highest OMC state predictions of 30 and 130MPa respectively, i.e. $E_0 = E_{max} = 30/130\text{MPa}$ and
- (ii) varying E_t for two cases of $30 \leq E_t \leq 80 \text{ MPa}$ and $80 \leq E_t \leq 130 \text{ MPa}$.

Fig. 5.16 shows the results of these four cases examined. Accordingly, it can be concluded that model output is very sensitive to E_0 and E_{max} . Whilst the effect of increasing E_0 is to increase the initial stiffness of the specimen, the effect of increasing E_{max} appears to be an increase in the remoulding capability of resistance to penetration.

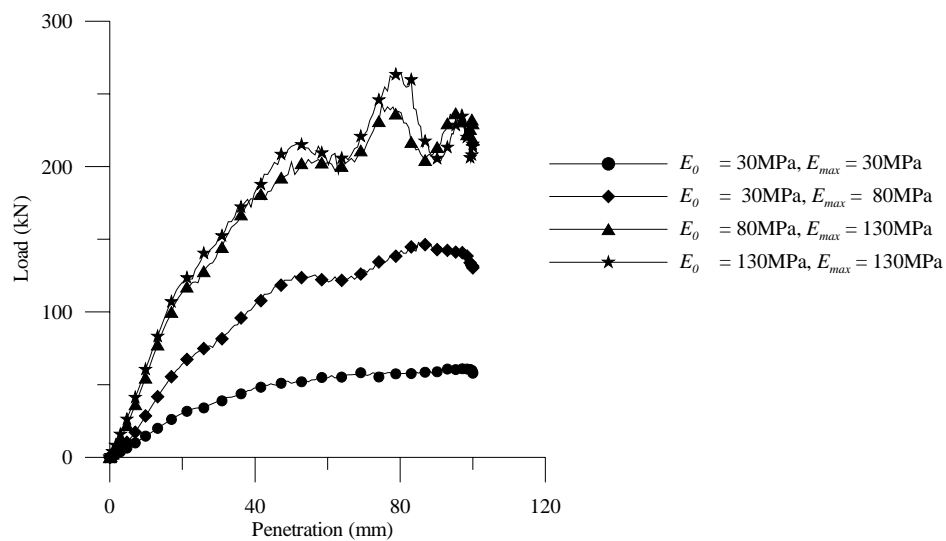


Figure 5.16 Effect of E_t : SCT Specimen Behaviour

As the variation in $35^\circ \leq \phi \leq 38^\circ$ for the OMC state was 3° , to understand the effect of friction angle ϕ to the load-penetration behaviour following cases were studied:

- (i) keeping ϕ as a constant, i.e. $\phi_{max} = \phi_{min} = 35^\circ$, and
- (ii) using two different ranges of ϕ , $25^\circ \leq \phi \leq 35^\circ$ and $35^\circ \leq \phi \leq 45^\circ$.

As the variation in the friction angle for one particular material cannot show very high values (more than 10^0), the difference between ϕ_{\max} and ϕ_{\min} were kept at 10^0 . It can be seen from the load-penetration profiles shown in Fig. 5.17, that there is not much variation in load-penetration profiles compared to the effect caused by E_r . Therefore, ϕ in its present form of usage as a pressure sensitive property is not a very sensitive input parameter for the current FE model. This may be considered as an advantage of the FE model as we do not have to pay significant attention in determining the values of ϕ_{\min} and ϕ_{\max} .

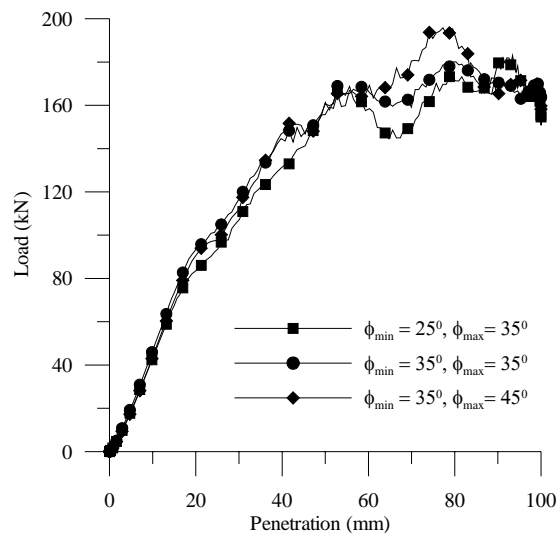


Figure 5.17 Effect of changes to ϕ : SCT Specimen Behaviour

Fig. 5.18 shows the effect of c . As the OMC state predictions showed low values for c (300 and 350kPa), three cases for the sensitivity were considered namely the average value of $c = 325\text{kPa}$, $c = 0.1\text{kPa}$, i.e. almost zero and $c = 1000\text{kPa}$. The effect was not prominent in the load-penetration profiles. Therefore, c is regarded as not particularly sensitive to the behaviour of capping layer.

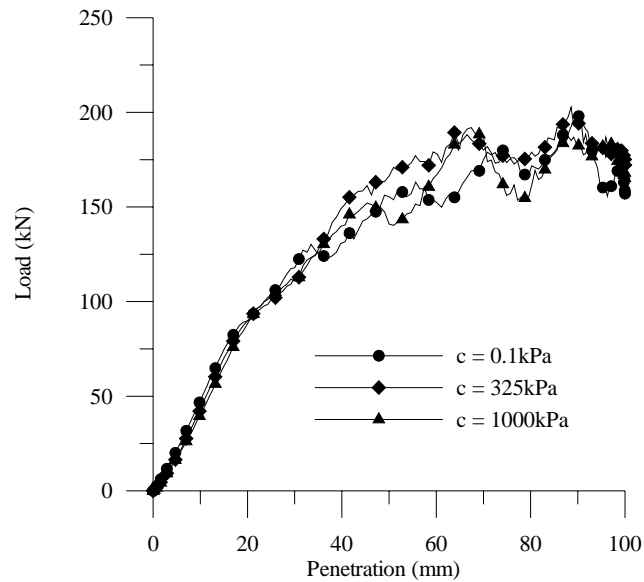


Figure 5.18 Effect of c : SCT Specimen Behaviour

Thus, from the sensitivity analysis of the elastic parameters it can be concluded that the tangent modulus is the most sensitive parameter; the friction angle and cohesion are very much less sensitive parameters. Care must therefore be taken in characterising the material properties E_0 and E_{max} .

2) Plastic parameters

The plastic parameters considered in the sensitivity analysis are ψ and H_p .

For associated flow rule $\phi = \psi$ and for non-associated flow rule $\phi \neq \psi$. If it is assumed that $35^\circ \leq \phi \leq 38^\circ$, then for the non-associated flow rule the ψ will have to be set as $0 \leq \psi \leq 35^\circ$ and for associated flow rule ψ has to be set as $35^\circ \leq \psi \leq 38^\circ$. Fig. 5.20 shows the load-penetration behaviour for non-associated flow rule for the cases of $\psi = 0^\circ$, $\psi = 5.5^\circ$ and $\psi = 34^\circ$. The higher the value of ψ , the higher is the resistance to penetration. Also note that the lower the difference between ϕ and ψ the higher is the

initial slope of the load-penetration profiles. Therefore ψ is regarded as a very sensitive plastic parameter.

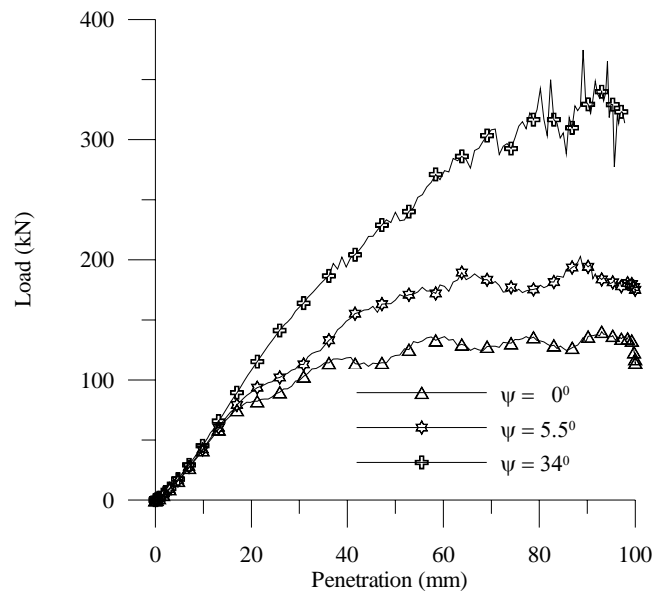


Figure 5.19 Effect of changes to ψ : SCT Specimen Behaviour

The sensitivity of H_p was observed by comparing the responses when $H_p = 0.0, 325,$ and 1000kPa considering values lower/higher than the average of the OMC state of 325kPa .

As shown in Fig. 5.21 the effect is not prominent compared to the sensitivity in ψ .

Therefore, H_p is considered not a very sensitive parameter.

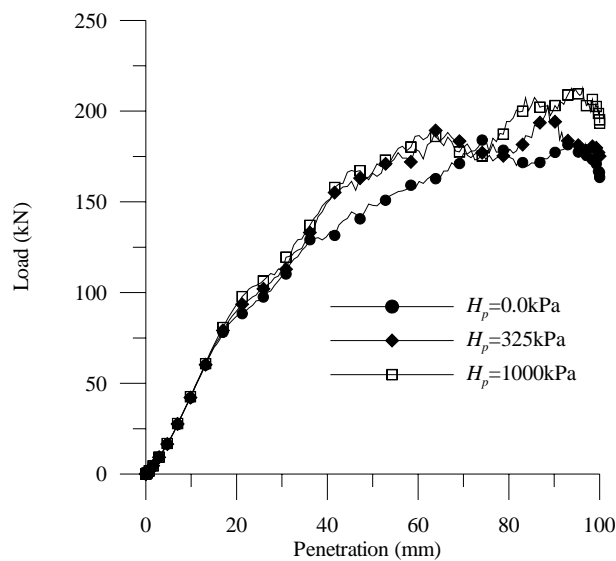


Figure 5.20 Effect of H_p : SCT Specimen Behaviour

Therefore, from the plastic parameters considered in the sensitivity analysis, the dilation angle was the most sensitive while hardening modulus is less sensitive in influencing predicted load-penetration profiles.

From the sensitivity analyses of the five input parameters considered in the backcalculation process it can be concluded that E_t and ψ are the most sensitive parameters. All other parameters showed insignificant sensitivity. Therefore care should be taken in the determination of the E_t and ψ values.

It can be further concluded from this parametric study that when performing an analysis of complex phenomenon like the nonlinear capping layer behaviour, care should be taken when assigning input values to the model. Though the above analysis was carried out varying only one parameter at a time so that its influence could be separated, care must be taken when assigning the model inputs as some parameters not considered to be sensitive (ϕ, c, H_p) when looked at individually may have a greater influence in the outcome of a combination.

5.3 Viability of the Model

The other main consideration is the viability of the model given the very high axial stress and confining stress induced in the semi-confined small scale mould used in the SCT. The normal and confining stresses induced at various penetration levels of the loading cylinder for a typical simulation are shown in Figs. 5.21 and 5.22 respectively. The corresponding FE analysis data are given in Appendix C.10.

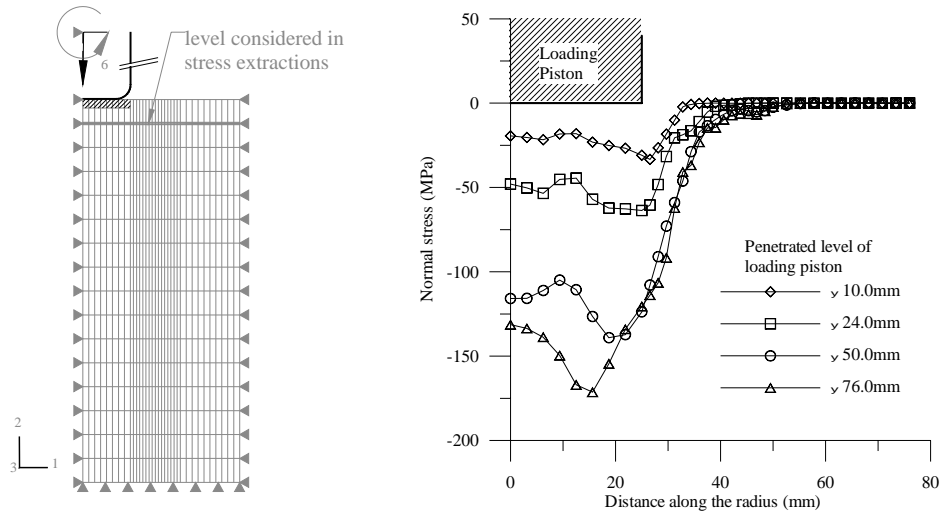


Figure 5.21 Normal stress development along a selected level with the penetration of the loading piston

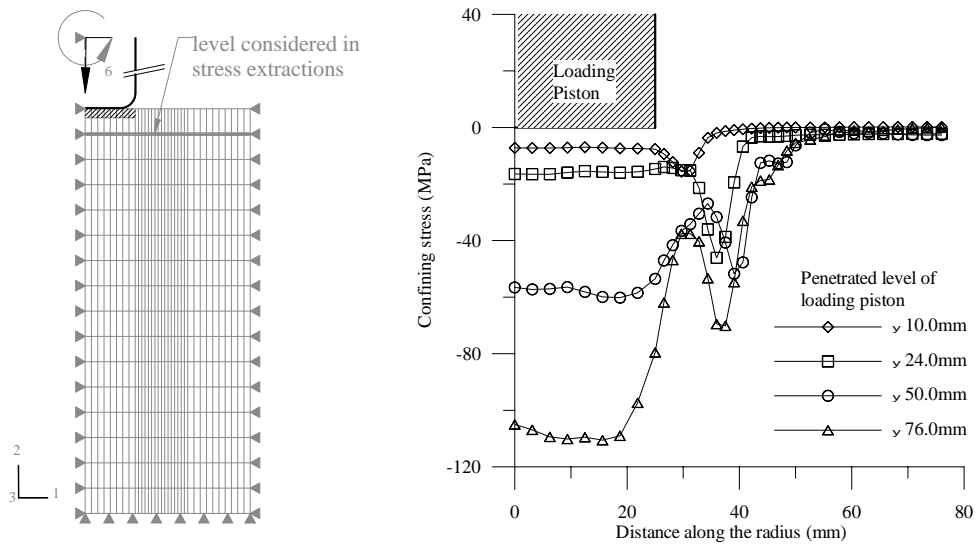


Figure 5.22 Confining stress development along a selected level with the penetration of the loading piston

It can be seen that even at a small penetration level of 10mm, the confining stresses are in excess of 1.0MPa. Even though the induced normal and confining stresses are high, by controlling E_0 and E_{max} suitably, reasonable material properties have been obtained using the backcalculation technique, thus vindicating the approach. Therefore it can be stated that the model is viable and can be used as a tool for the prediction of material properties.

The viability of the model for application to actual practical cases in the field will differ as the confining stresses induced in an infinite soil mass will be very much smaller compared to the stresses induced in the small scale SCT setup where the boundary effects influence the material behaviour. This issue is dealt with in Chapter 6 which discusses how the model was changed to suit plane strain conditions, and its behaviour is tested in a purpose built large scale experimental setup.

5.4 Summary

This Chapter has described a new user defined material routine for ABAQUS/Explicit simulations which incorporates a pressure dependent modulus and a friction angle. The capping layer material has successfully been characterised by the ABAQUS/Explicit model. The backcalculated material parameters have been compared with general soil properties published and triaxial/uniaxial test data.

The model was able to predict the material properties considering a wider range of stress levels as well as saturation levels adopted in the testing. Thus, it provided valuable representation of data more broadly than for a single stress-level/saturation condition or restricted narrow ranges of stress-levels/saturation conditions.

Six material parameters (the tangent modulus, Poisson's ratio, friction angle, cohesion, dilation angle and hardening modulus) were obtained from the backcalculation process whereas the current level of knowledge in inverse technique could not predict more than four parameters successfully. The model was able to predict satisfactory ranges for the

“engineering material parameters” rather than predicting singular values as soil is a very complex medium with a great level of variability.

The saturation level has the most significant effect on material properties. The elastic material properties of tangent modulus, friction angle and cohesion reduced with the increase in the moisture content. The plastic properties of dilation angle and the hardening modulus increased with the increase in the moisture.

The parametric study showed that tangent modulus and dilation angle are the most sensitive when looked at individually. However, choice of appropriate input parameters is of importance for any numerical analysis and sound knowledge of the effect of input parameters on the expected results will considerably improve the sensibility and reliability of the results.

It is expected that the implementation of the ABAQUS/Explicit model for advanced railway substructure structural response analysis will lead to better understanding of railway substructure and will be presented in Chapter 6.